INSIGHTS ON THE MECHANISMS OF SEAWATER-MIXING CALCIUM SILICATE SLAG-BASED ALKALI-ACTIVATED MATERIALS

DI SHI[1,2], JIAYUAN YE[2], WENSHENG ZHANG[2]*, WEIGUO SHEN[1]
[1] *State Key Laboratory of Silicate Materials for Architecture, Wuhan University of Technology, Wuhan 430070, China*
[2] *State Key Laboratory of Green Building Materials, China Building Materials Academy, Beijing 100024, China*

In order to get a full understanding of the mechanisms of seawater-mixing alkali-activated materials, calcium silicate slag (CSS)-based alkali-activated materials (AAMs) with various content of Cl^- were synthesized, and then the effect of Cl^- on the properties, products, hydration heat evolution, microstructure of AAMs, as well as the characteristics of alkaline solution were investigated. The results showed that the Cl^- introduced in the form of solid NaCl significantly decreased the mechanical properties of CSS-based AAMs in the range higher than 1 wt%. This properties degradation can be attributed to the hydration inhibitions caused by the dissolution of solid NaCl and the interaction between NaCl and sodium silicate solution, as well as the formation of non-cementitious sodalite other than C(N)-A-S-H gels. Despite this, the findings of this study provided further evidence for the application potentialities of seawater in AAMs as mixing water due to the limited content of Cl^- in seawater.

Keywords: *calcium silicate slag; alkali-activated materials; Cl^-; interaction; seawater-mixing*

1. Introduction

Seawater and sea sand are strictly forbidden in reinforced concrete due to the risks of steel corrosion caused by Cl^- [1]. Therefore, constructions in marine environments have higher costs as compared with those in land environments due to the limited resources like freshwater and suitable sand.

In fact, the depassivation of steels in concrete is dependent on the [Cl^-/OH^-] ratio other than the simple Cl^- concentration of the pore solution [2, 3]. In consideration of the fact that the chlorinity of seawater is only about 1.8% and other ions in seawater might be favorable to the early hydration of cement, there are great potentialities for the utilization of seawater in high-alkalinity concretes as mixing water [4-7].

Alkali-activated materials (AAMs), composed of alkali sources and aluminosilicate precursors, are considered promising substitutions to ordinary Portland cement (OPC) in order to reduce CO_2 emissions and reutilize solid wastes [8-10]. Besides the high alkalinity, AAMs are believed to have better chloride binding ability than OPC due to the formation of low Ca/Si ratio C(N)-(A)-S-H gels or Cl^- containing products [1, 11-13], enabling the utilization of seawater in AAMs as mixing water.

The studies in the past years have confirmed the huge potentialities of seawater-mixing AAMs [7]. However, the effects of seawater on the properties of AAMs varied significantly in different studies. Some researchers found that the mixing of seawater had negligible effects on the strengths of AAMs [14], while the acceleration/inhibition effects were detected in the alkali-activation process and property developments of seawater-mixing AAMs in some other studies [13, 15-18]. The effects of seawater-mixing are complicated, and the presence of different salts in seawater is believed to be one of the main reasons besides the various raw materials.

The authors previously investigated the properties, mineralogy, and microstructure of seawater-mixing calcium silicate slag (CSS)-based AAMs, and found that seawater-mixing slightly decreased the strengths of CSS-based AAMs. This strength decrease was attributed to the ion exchange reaction between the Mg^{2+} from seawater and the silicate anions from liquid sodium silicate to produce amorphous M-S-H gels and SiO_2 gels [19]. However, the effects of other ions, especially the Cl^-, on the alkali-activation and the related mechanisms are still unacknowledged.

In order to fully understand the mechanisms of seawater-mixing AAMs, the CSS-based AAMs with various content of Cl^- were synthesized in this study. Then, the influence of Cl^- on the characteristics of alkaline solution, as well as the properties, reaction products, hydration, and microstructure were investigated. The findings provided further insights into the mechanisms of seawater-mixing CSS-based AAMs.

2. Experimental materials and methods

2.1. Materials

Original CSS was obtained from Inner Mongolia Datang International Hohhot Aluminum-electricity Co., Ltd, China. The original CSS was dried at 105℃ for 24 h and then grounded to obtain the dried CSS powder. Commercial GGBFS was purchased from Shanghai Baotian New Building Materials Co., Ltd, China. Class F fly ash (FA) was obtained from Henan Xing'an New Building

*Autor corespondent/*Corresponding author*,
E-mail: wensheng_zhang01@163.com

Table 1

Chemical composition of raw materials / *wt%*

Compositions	CaO	SiO_2	Al_2O_3	Fe_2O_3	MgO	K_2O	Na_2O	SO_3	LOI*	∑
CSS	48.3	25.3	7.4	2.6	2.4	0.3	3.3	0.6	8.8	99.0
GGBFS	37.9	33.5	12.5	1.1	9.3	-	-	2.5	-	96.8
FA	3.9	42.9	41.3	4.3	0.6	-	-	0.2	1.3	94.5

* - Loss on ignition.

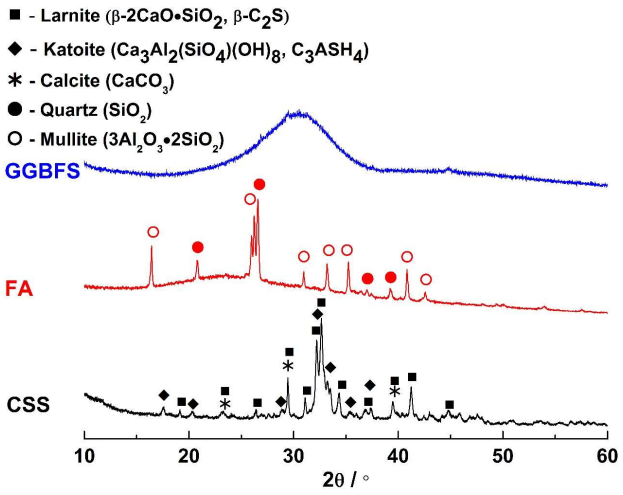

Fig. 1 - XRD patterns of raw materials

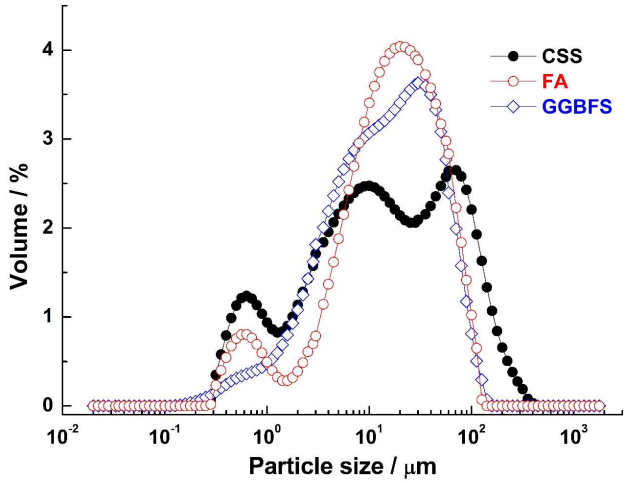

Fig. 2 - Particle size distributions of raw materials

Materials Co., Ltd, China. The chemical composition of raw materials is shown in Table 1.

From the XRD patterns of raw materials, as shown in Fig. 1, it can be seen that CSS mainly consists of crystalline phases like larnite (β-C_2S), calcite ($CaCO_3$), and katoite ($Ca_3Al_2(SiO_4)(OH)_8$, C_3ASH_4). By contrast, FA is mainly composed of crystalline quartz (SiO_2), mullite ($3Al_2O_3•2SiO_2$), and amorphous glass, while GGBFS is mostly comprised of the vitreous phase.

The particle size distributions of CSS, GGBFS, and FA are given in Fig. 2. There is only one peak detected in the particle distribution curve of GGBFS, while CSS exhibited the widest particle distribution.

The ISO quartz sand from Xiamen ISO Standard Sand Co., Ltd. was selected as the fine aggregate in mortars.

Technical grade liquid sodium silicate containing 31.73 wt% of SiO_2, 13.65 wt% Na_2O, and 54.62 wt% of H_2O was purchased from Beijing red star chemical building materials Co., Ltd. The mass ratio of Na_2O to H_2O was adjusted to 1/10 by adding a certain content of freshwater into the liquid sodium silicate. Then, the alkaline solution was homogeneously stirred and stored in a sealed container at room temperature for at least 24 h before use.

In order to avoid the effects of other ions, solid analytical reagent sodium chloride (NaCl with purity ≥ 99.5%), purchased from Sinopharm Chemical Reagent Co., Ltd., was used as the additive for the introduction of Cl^- in this study.

2.2. Specimen preparation

As shown in Fig. 3, the CSS-GGBFS-FA blend was firstly premixed with a CSS: GGBFS: FA mass ratio of 52.5: 22.5: 25.0 according to previous studies [19, 20]. It should be noted that the natural seawater contains about 3.5 wt% salts, which are mainly composed of NaCl. This implies that the Cl^- content of seawater is only about 2.0%. The limited content makes it difficult to identify the effects of Cl^- in seawater-mixing AAMs. Thus, a series Cl^- content up to 5.0 wt% (calculated by the mass ratio of the CSS-GGBFS-FA blend) was designed in this study (Table 2). Taking into consideration that the Cl^- was introduced in the form of NaCl, the certain content of solid NaCl was homogenously premixed with the CSS-GGBFS-FA blend in this study. Then, the CSS-based alkali-activated materials with various content of Cl^- were synthesized by mixing the blend and the alkaline solution. The mass ratio of water to CSS-GGBFS-FA blend (W/B) was set as 0.50 for all the mixtures. The pastes sizing 40 mm × 40 mm × 40 mm were prepared following the Chinese standard GB/T 1346-2011 [21] for the mineralogical analyses of reaction products. The mortars sizing 40 mm × 40 mm × 160 mm were prepared in accordance with the Chinese standard GB/T 17671-1999 [22] and used for the mechanical properties tests and microstructure analyses. The specimens were immediately transferred into a curing cabinet at 20 ± 1°C, RH ≥ 95%. After 24 h, the specimens were demolded and transferred back to the curing cabinet until testing ages.

2.3. Test methods

The specimens were taken out from the curing cabinet at 3 days and 28 days, respectively. The mechanical properties of mortars including flexural

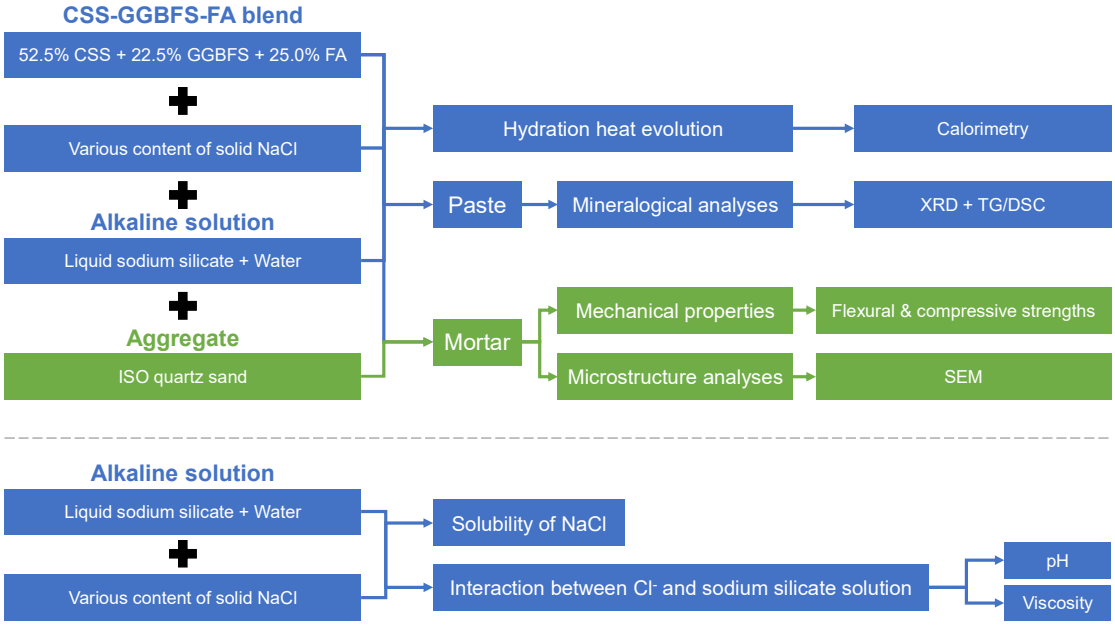

Fig. 3 – Experimental diagram

Table 2

Mixture design of CSS-based AAMs with various content of Cl^- / wt%

No.	Content of Cl^-*	Content of Na^+*
Control	0.0	0.0
C1	1.0	0.7
C2	2.0	1.3
C3	3.0	2.0
C4	4.0	2.6
C5	5.0	3.3

* - by the mass ratio of the CSS-GGBFS-FA blend.

and compressive strengths were tested using a TYE-300D anti-fold and compression testing machine (Three replicates per data of flexural strength and six replicates per data of compressive strength). The pastes and the tested mortars were crushed into pieces with a hammer, and immediately immersed in ethanol for 24 h to stop the further alkali-activation. The mortar pieces were dried in a vacuum oven at 45℃ and -0.08 MPa for 48 h before the microstructure analyses. The paste pieces were dried with the same procedure and grounded with an agate mortar for 10 min before the mineralogical analyses.

The X-ray diffraction patterns were recorded using a Bruker D8 automated diffractometer (Cu-K_α radiation). The tests were performed in the range of 5º - 65º at a step size of 0.02º and a scanning rate of 8 º/min (2θ). The comprehensive thermal analyses (TG/DSC) were conducted with NETZSCH STA 449C from 30℃ to 1000℃ at a heating rate of 10 ℃/min in N_2 atmosphere. The microstructure analyses were carried out on FEI Quanta 250 FEG *Scanning Electron Microscope (SEM) at 20 kV*. The hydration heat analyses were run using a TAM Air Calorimetry at 20℃ with the same W/B ratio of 0.50 over the first 72 h of reaction.

In addition, although the analytical reagent NaCl was selected to avoid the effects of other ions in this study, the Na^+ introduced concomitantly with Cl^- would inevitably change the characteristics of the alkaline solution due to the nonnegligible content (Table 2). On the other hand, despite that NaCl is readily soluble in H_2O, the large amount of Na^+ in the alkaline solution might also have an impact on the dissolution behavior of NaCl. Therefore, in order to get a full understanding of the mechanisms of Cl^-, alkaline solutions with various content of Cl^- were also prepared and stored in sealed plastic bottles at room temperature. After 24 h, the pH values of these alkaline solutions were tested using a Sartorius PB-10 pH Meter, and the viscosities were measured with a Lichen NDJ-9S rotational viscometer. As shown in Fig. 4, the transparent alkaline solutions with various content of Cl^- indicated the complete dissolution of NaCl in this study.

3. Results and discussion

3.1. Mechanical properties

The mechanical properties (including flexural and compressive strengths) of CSS-based AAMs with various content of Cl^- are presented in Table 3.

The flexural strength of the control reached 4.1 MPa and 7.4 MPa at 3 days and 28 days, respectively. At the same time, the compressive strength of the control reached 26.7 MPa at 3 days and 57.4 MPa at 28 days. As 1 wt% Cl^- was introduced, the flexural strength of CSS-based

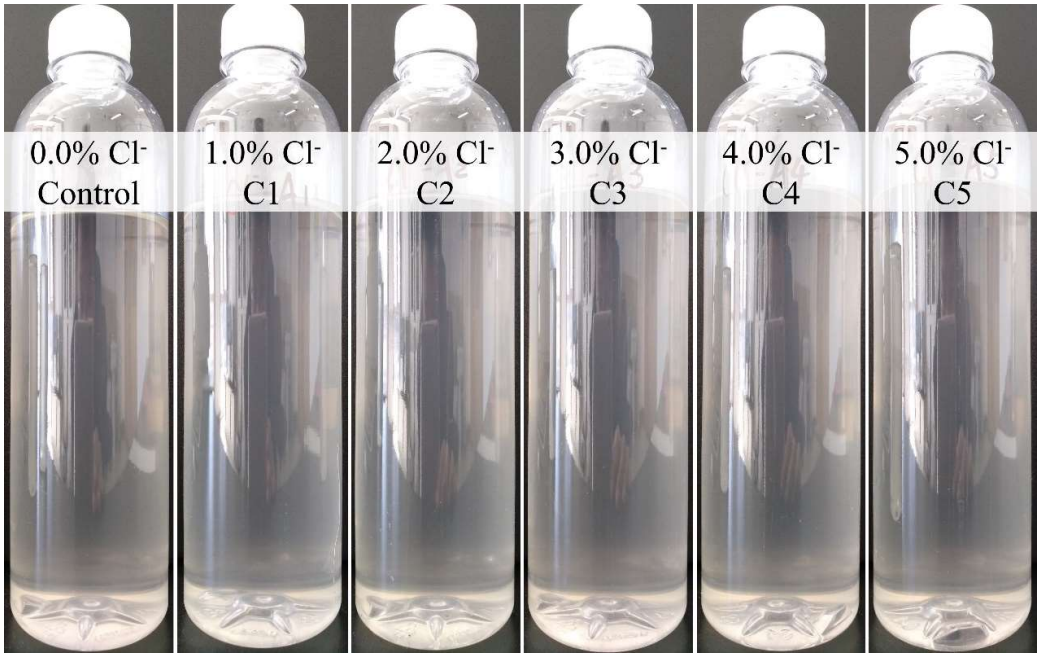

Fig. 4 – Alkaline solutions with various content of Cl^-

Table 3

Mechanical properties of CSS-based AAMs with various content of Cl^-

No.	Content / wt%		Flexural strength / MPa		Compressive strength / MPa	
	Cl^-	Na^+	3d	28d	3d	28d
Control	0.0	0.0	4.1	7.4	26.7	57.4
C1	1.0	0.7	3.0	5.8	9.0	53.6
C2	2.0	1.3	/	/	/	13.0
C3	3.0	2.0	/	/	/	3.8
C4	4.0	2.6	/	/	/	3.2
C5	5.0	3.3	/	/	/	/

/ - The value of the strength was beyond the lower limit of the testing machine.

AAMs slightly decreased. By contrast, a significant reduction was detected on the compressive strength at 3 days, while the compressive strength at 28 days only marginally decreased. As the content of Cl- exceeded 1 wt%, remarkable strength reduction was observed on the mechanical properties of CSS-based AAMs. Especially, the flexural strength and the compressive strength at 3 days had completely deteriorated. This strength degradation indicated the significant effects of NaCl on the alkali-activation of CSS-based AAMs, which will be explained through the analyses of reaction products, hydration heat and microstructure next.

3.2. Reaction products

3.2.1. XRD analyses

The XRD patterns of CSS-based AAMs with various content of Cl^- are given in Fig. 5.

The control mainly consisted of crystalline phases like larnite, katoite, quartz and mullite, which derived from the unreacted raw materials. It should be noted that the main reaction products of CSS-based AAMs are amorphous C(N)-A-S-H gels according to previous studies [19, 20, 23]. This explained the phenomenon that there were no other crystalline phases detected in the control.

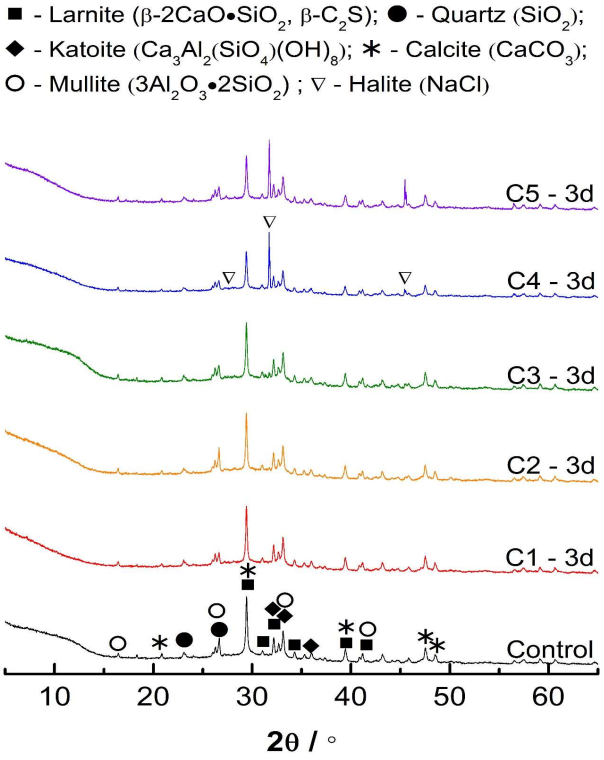

Fig. 5(a) - XRD patterns of CSS-based AAMs with various content of Cl^- - 3d

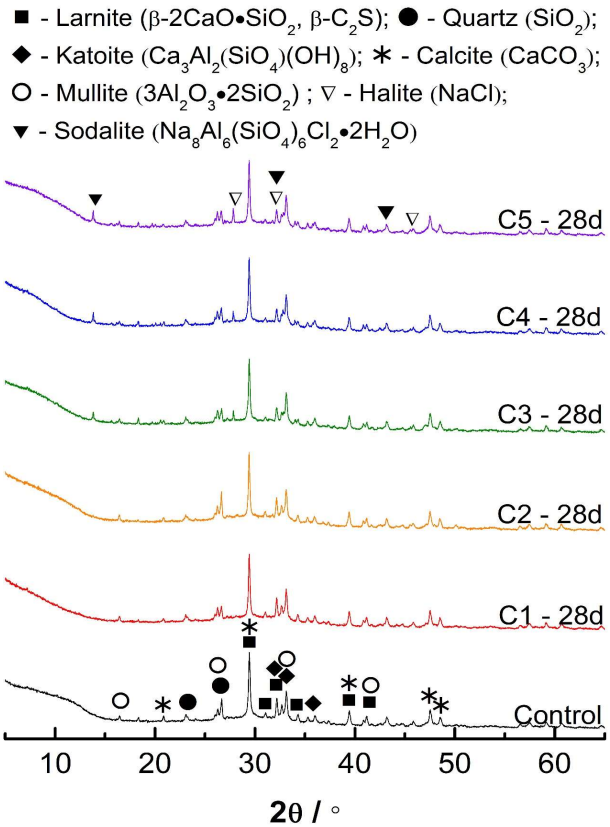

Fig. 5(b) - XRD patterns of CSS-based AAMs with various content of Cl^- - 28d

As the content of Cl^- was lower than 3 wt%, the mineralogy of CSS-based AAMs barely changed. This might be attributed to the limited content of NaCl or reaction products. As the content of Cl^- exceeded 3 wt%, the typical peaks characteristic of halite (NaCl) were detected in the XRD patterns of CSS-based AAMs. This provided evidences for the inference that only limited Cl^- participated into the alkali-activation at 3 days.

The CSS-based AAMs with low content of Cl^- (≤2 wt%) exhibited similar XRD patterns as the control at 28 days. However, the typical peaks of sodalite ($Na_8Al_6(SiO_4)_6Cl_2•2H_2O$) were observed as the content of Cl^- was higher than 2 wt%, indicating the formation of sodalite in CSS-based AAMs with Cl^-. The non-cementitious sodalite produced in the system is one of the reasons for the significant strength deterioration caused by the Cl^-.

3.2.2. TG/DSC analyses

The TG/DSC curves of CSS-based AAMs with various content of Cl^- are shown in Fig. 6. Two endothermic peaks with obvious weight loss and one exothermic peak with neglectable weight loss were detected in the TG/DSC curves of the control at 3 days. The endothermic peaks centered at around 120℃ is generally assigned to the evaporation of *f*-H_2O [24]. The endothermic peak with significant weight loss at around 700℃ is assigned to the decomposition of $CaCO_3$ into CaO and CO_2. The exothermic peak at about 820℃ is

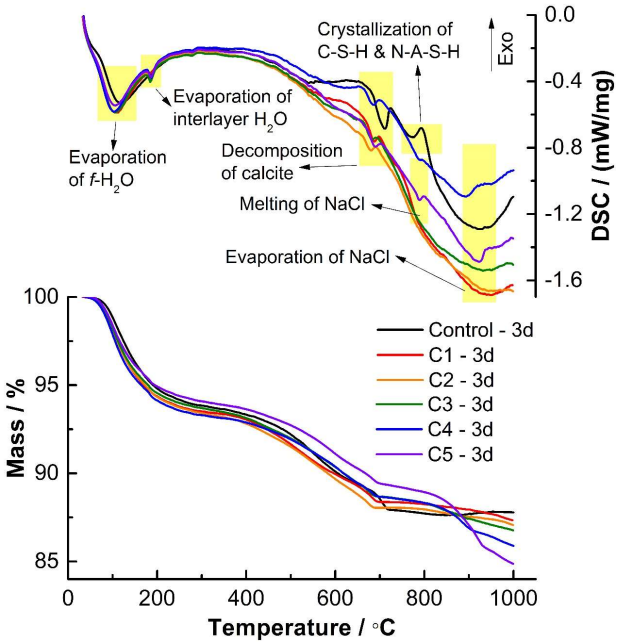

Fig. 6(a) - TG/DSC curves of CSS-based AAMs with various content of Cl^- - 3d

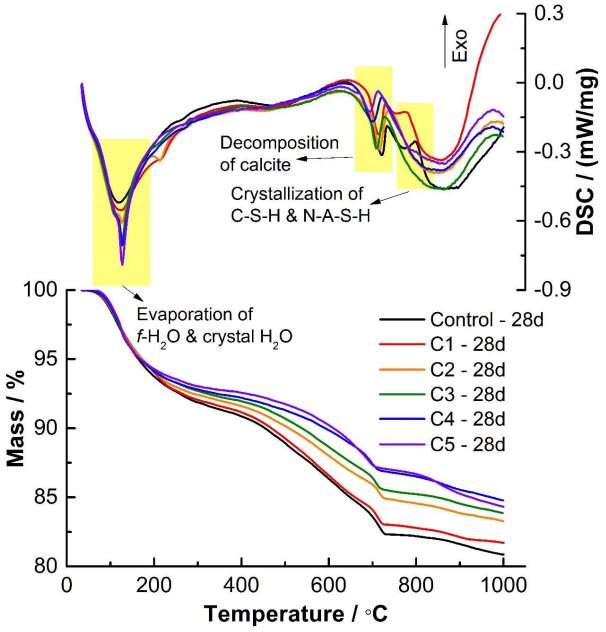

Fig. 6(b) - TG/DSC curves of CSS-based AAMs with various content of Cl^- - 28d

attributed to the crystallization of amorphous C-S-H gels to β-wollastonite and N-A-S-H gels to carnegieite or nepheline [20, 25].

As various content of Cl^- was introduced into CSS-based AAMs, the peaks characteristic of the evaporation of H_2O and the decomposition of $CaCO_3$ barely changed at 3 days. However, a small endothermic peak centered at around 260℃, which is generally related with the evaporation of interlayer H_2O, is observed in the TG/DSC curves of CSS-based AAMs. Besides, the peaks assigned to the crystallization of C-S-H/N-A-S-H gels disappeared. Especially, as the content of Cl^-

exceeded 3 wt%, two endothermic peaks, one with light weight loss centered at around 800℃ and another with significant weight loss at about 900℃, were detected in the TG/DSC curves of CSS-based AAMs. According to the XRD results obtained above, these two peaks can be attributed to the melting and evaporation of unreacted NaCl, respectively [26].

The control exhibited similar TG/DSC curves as the curing age extended to 28 days. However, distinct changes can be detected in the TG/DSC curves of CSS-based AAMs with various content of Cl^-. Firstly, the peaks characteristic of the melting and evaporation of NaCl disappeared, indicating the complete reaction of NaCl at 28 days. Secondly, the crystallization peak of C-S-H/N-A-S-H gels can be obviously detected in the TG/DSC curves of CSS-based AAMs with 1 wt% Cl^-. Nevertheless, this peak disappeared as the content of Cl^- was further increased, which is consistent with the strength results mentioned above. Besides, the peaks characteristic of the melting and evaporation of NaCl were not observed. Meanwhile, a sharp endothermic peak with wight loss centered at 126℃, which is generally assigned to the evaporation of crystal H_2O, was detected. Based on the XRD results obtained, it can be inferred that this peak is attributed to the crystal H_2O evaporation of sodalite. This provided further evidences for the production of sodalite in CSS-based AAMs with Cl^-.

3.3. Hydration heat evolution

The hydration heat evolution of CSS-based AAMs with various content of Cl^- is shown in Fig. 7. There were four peaks detected in the hydration heat evolution curve of the control. The initial peak (Peak 1) in first few minutes is related with the heat of rapid wetting and dissolution of raw materials. The two initial additional peaks (Peak 2 and Peak 3) can be attributed to the reaction between anions/anion groups from alkaline solution and dissolved Ca^{2+} from raw materials, in this study which were C_2S and GGBFS, respectively. The accelerated hydration peak (Peak 4) is assigned to the further hydration of raw materials [23].

As various content of Cl^- was introduced into CSS-based AAMs, the hydration was significantly inhibited, which was reflected on the hydration peak shift to later ages and the peak intensity decrease with the content of Cl^-. The Cl^- was introduced in the form of solid NaCl in this study. In consideration of the fact that the dissolution of NaCl is an endothermal process, this phenomenon can be attributed to the effects of NaCl dissolution. It is well known that the temperature plays a vital role in the chemical reaction. The rate of a chemical reaction will be doubled with a temperature increase of every 10℃ [27]. There is no doubting the temperature decrease of the system due to the dissolution of solid NaCl. Thus, this might be one of the reasons

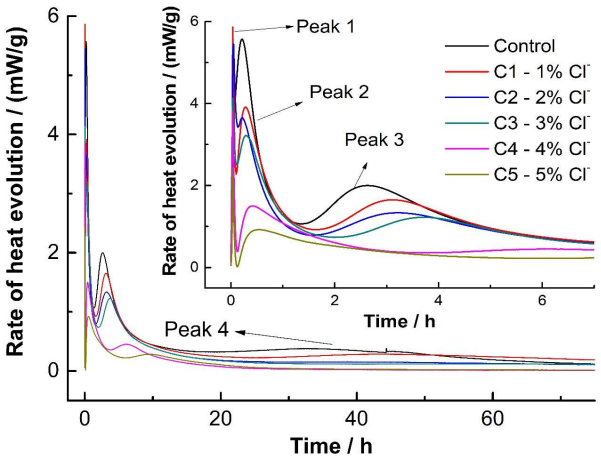

Fig. 7 – Hydration heat evolution of CSS-based AAMs with various content of Cl^-

for the hydration inhibition of CSS-based AAMs with Cl^-.

Besides, the alkalinity and the silicate anions composition of alkali silicate solution is regarded as one of the key factors in alkali-activation by determining the dissolution of raw materials and the formation of initial C-S-H gels [27]. The sodium silicate solution with a Na_2O/SiO_2 mass ratio of 1/10 was used in this study. The effects of Na^+ introduced concomitantly with Cl^- on the pH value and the ionic composition of the alkaline solution might be another reason for the hydration inhibition of CSS-based AAMs with Cl^-.

3.4. Microstructure

The micrographs of CSS-based AAMs with various content of Cl^- at 28 days are presented in Fig. 8. The control exhibited a dense matrix due to the formation of large amount of C(N)-A-S-H gels. As 1 wt% Cl^- was introduced, the CSS-based AAMs presented a comparative density as the control. However, the amount of C(N)-A-S-H gels significantly decreased as the content of Cl^- was further increased, consequently resulting into a more and more loose structure. This is consistent with the results of mechanical properties mentioned above.

3.5. Mechanisms of seawater-mixing

3.5.1 Interaction between Cl^- and sodium silicate solution

The viscosity and pH value of alkaline solutions with various content of Cl^- are presented in Fig. 9. The pH value of the alkaline solution gradually decreased from 12.15 to 11.70 with the Cl^- content from 0 wt% to 5 wt%. Generally, NaCl is considered as neutral salt due to the strong polarity of Na^+ and Cl^-. Thus, the addition of NaCl is assumed to have little effect on the pH value of the alkaline solution. However, the ions (Na^+ and silicate anions) in the alkaline solution derived from

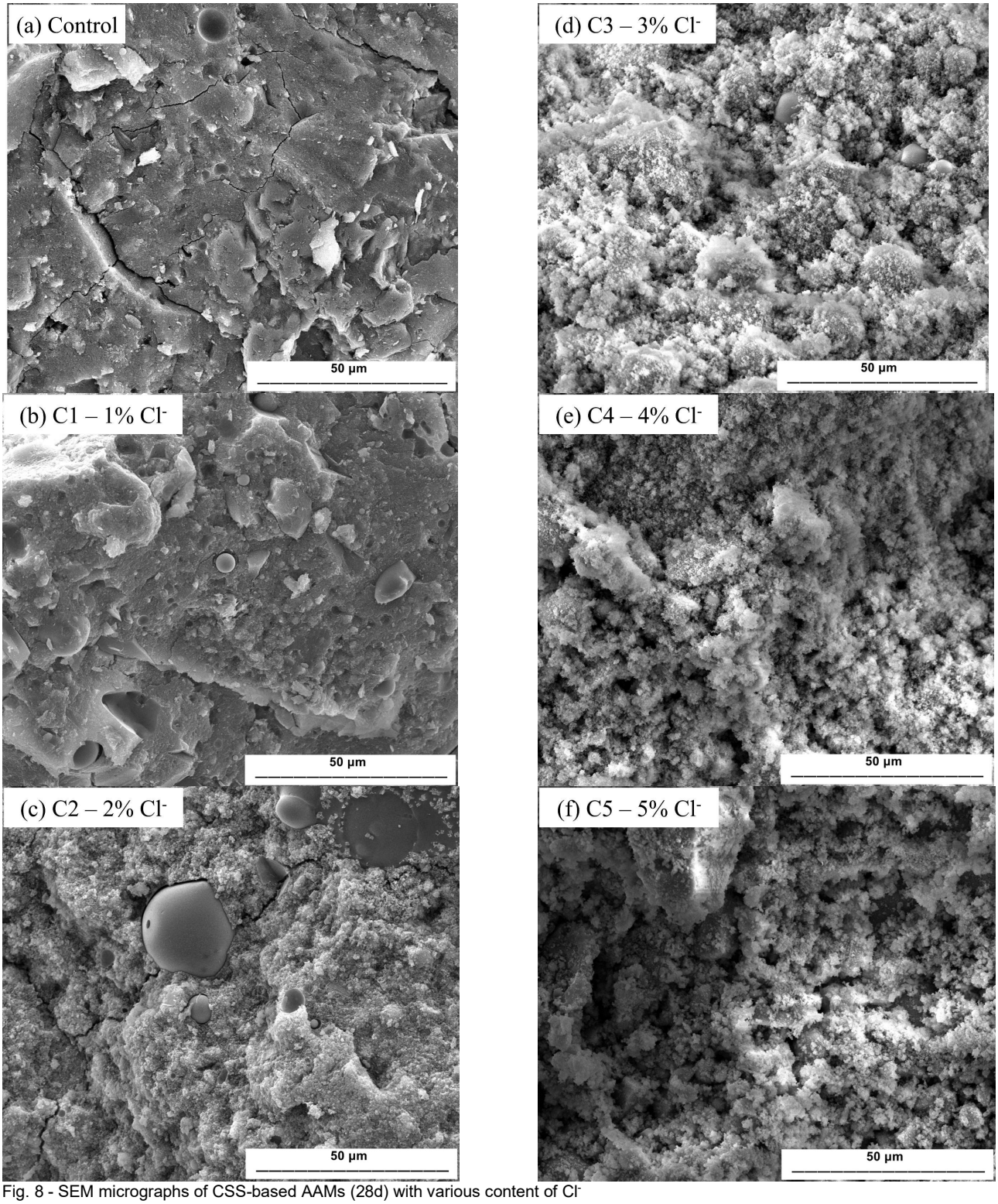

Fig. 8 - SEM micrographs of CSS-based AAMs (28d) with various content of Cl^-

the dissolution and the ionization of sodium silicate [27]. The addition of extra Na^+ would inevitably break the charge balance and inhibit the ionization of sodium silicate, consequently resulted into the pH decrease of the alkaline solution.

On the contrary, the viscosity of the alkaline solution progressively increased from 10.0 mPa•s to 15.5 mPa•s with the Cl^- content. The viscosity of inorganic salt solution is dependent on a series factors like salinity and the composition. It is well acknowledged that the viscosity of saline solution increases with the concentration of the ions [27, 28]. The addition of Cl^- and extra Na^+ markedly increased the ion concentration of the alkaline solution. This was one of the reasons for the viscosity increase. Besides, the introduction of other ions broke the balance between Na^+ and silicate anions, and subsequently contributed to the gelation of silicate anions [29,30]. Thus, the gelation of silicate anions caused by the introduction of Cl^-

and extra Na^+ might be another reason for the viscosity increase of alkaline solutions.

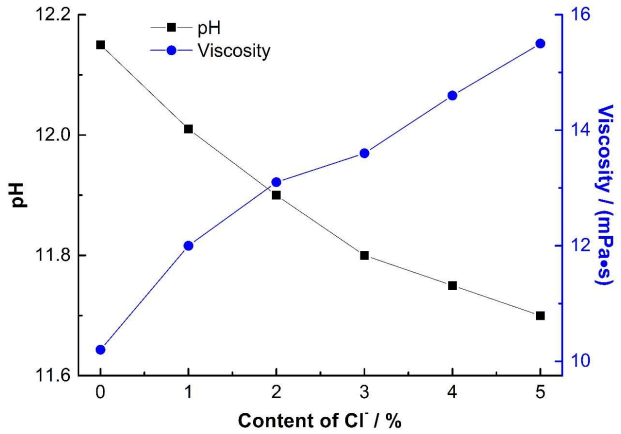

Fig. 9 – Viscosity and pH values of alkaline solutions with various content of Cl^-

3.5.2 Discussion on the effects of Cl^- from seawater

The results obtained above showed the Cl^- induced mechanical properties deterioration of CSS-based AAMs, which was much more significant as the Cl^- content exceeded 1 wt%. This deterioration can be explained by the temperature-induced hydration inhibition due to the dissolution of solid NaCl, the pH-dominated hydration inhibition due to the interaction between NaCl and sodium silicate solution, as well as the production of non-cementitious sodalite other than C(N)-A-S-H gels.

Generally, the concentration of Cl^- in seawater is about 1.9 wt%. Therefore, it can be deduced that the actual content of Cl^- in the seawater-mixing AAMs with a W/C ratio of 0.5 is less than 0.95 wt%. The Cl^- in this content range would markedly inhibit the mechanical properties development of AAMs at early ages. However, there is no dissolution process of solid NaCl in seawater-mixing AAMs. Besides, the content of Cl^- in AAMs would be much lower than 0.95 wt% as using liquid alkaline activators. This further evidenced the potentialities of seawater-mixing AAMs.

4. Conclusions

The mechanical properties, reaction products, hydration heat evolution and microstructure of CSS-based AAMs with various content of Cl^- were studied, and the mechanisms of seawater-mixing were discussed in this study. Based on the results obtained, the conclusions could be drawn as follows:

(1) As Cl^- was introduced in the form of solid NaCl, the mechanical properties of CSS-based AAMs significantly decreased with the content of Cl^- from 1 wt% to 5 wt%.

(2) The interaction between NaCl and sodium silicate solution resulted into the pH decrease and the viscosity increase of the alkaline solution.

(3) The properties degradation of CSS-based AAMs can be explained by the temperature-dominated hydration inhibition caused by the dissolution of solid NaCl, the pH dominated hydration inhibition caused by the interaction between NaCl and sodium silicate solution, as well as the production of non-cementitious sodalite other than C(N)-A-S-H gels.

Despite of the deteriorating effects of Cl^- on the properties, the limited salinity of seawater resulted into the extremely low concentration of Cl^- in seawater-mixing AAMs, providing further evidences for the potentialities of using seawater as mixing water of AAMs. However, there are more work (E.g. the effects of Cl^- from seawater on the steel corrosion behavior of reinforced alkali-activated concrete) to be done in the future.

Acknowledgements

The authors would like to thank the financial supports from State Key Laboratory of Silicate Materials for Architecture (Wuhan University of Technology) (SYSJJ2020-13), Natural Science Foundation of Beijing (2202061), and National Natural Science Foundation of China (51402279).

REFERENCES

[1] W. Tahri, X. Hu, C. Shi, Z. Zhang, Review on corrosion of steel reinforcement in alkali-activated concretes in chloride-containing environments, Constr. Build. Mater., 2021, **293**, 123484.

[2] S. Mundra, M. Criado, S.A. Bernal, J.L. Provis, Chloride-induced corrosion of steel rebars in simulated pore solutions of alkali-activated concretes, Cem. Concr. Res., 2017, **100**, 385-397.

[3] M.S.H. Khan, O. Kayali, Chloride binding ability and the onset corrosion threat on alkali-activated GGBFS and binary blend pastes, European Journal of Environmental and Civil Engineering, 2016, **22**(8), 1023-1039.

[4] H. Li, N. Farzadnia, C. Shi, The role of seawater in interaction of slag and silica fume with cement in low water-to-binder ratio pastes at the early age of hydration, Constr. Build. Mater., 2018, **185**, 508-518.

[5] A. Younis, U. Ebead, P. Suraneni, A. Nanni, Fresh and hardened properties of seawater-mixed concrete, Constr. Build. Mater., 2018, **190**, 276-286.

[6] D. Pan, S.A. Yaseen, K. Chen, D. Niu, C.K. Ying Leung, Z. Li, Study of the influence of seawater and sea sand on the mechanical and microstructural properties of concrete, J. Build. Eng., 2021, **42**, 103006.

[7] U. Ebead, D. Lau, F. Lollini, A. Nanni, P. Suraneni, T. Yu, A review of recent advances in the science and technology of seawater-mixed concrete, Cem. Concr. Res., 2022, **152**, 106666.

[8] S.S. Mohapatra, J. Mishra, B. Nanda, S.K. Patro, A review on waste-derived alkali activators for preparation of geopolymer composite, Materials Today: Proceedings, 2022, **56**, 440-446.

[9] V. Ponomar, J. Yliniemi, E. Adesanya, K. Ohenoja, M. Illikainen, An overview of the utilisation of Fe-rich residues in alkali-activated binders: Mechanical properties and state of iron, J. Cleaner Prod., 2022, **330**, 129900.

[10] A. Alsalman, L.N. Assi, R.S. Kareem, K. Carter, P. Ziehl, Energy and CO_2 emission assessments of alkali-activated concrete and Ordinary Portland Cement concrete: A comparative analysis of different grades of concrete, Clean. Environ. Syst., 2021, **3**, 100047.

[11] Y. Jun, T. Kim, J.H. Kim, Chloride-bearing characteristics of alkali-activated slag mixed with seawater: Effect of different salinity levels, Cem. Concr. Compos., 2020, **112**, 103680.

[12] J. Zhang, C. Shi, Z. Zhang, Chloride binding of alkali-activated slag/fly ash cements, Constr. Build. Mater., 2019, **226**, 21-31.

[13] Y. Jun, J.H. Kim, S.H. Han, T. Kim, Influence of seawater on alkali-activated slag concrete, Mater. Struct., 2021, **54**(3), 121.
[14] S. Yang, J. Xu, C. Zang, R. Li, Q. Yang, S. Sun, Mechanical properties of alkali-activated slag concrete mixed by seawater and sea sand, Constr. Build. Mater., 2019, **196**, 395-410.
[15] W. Lv, Z. Sun, Z. Su, Study of seawater mixed one-part alkali activated GGBFS-fly ash, Cem. Concr. Compos., 2020, **106**, 103484.
[16] A.M. Rashad, M. Ezzat, A Preliminary study on the use of magnetic, Zamzam, and sea water as mixing water for alkali-activated slag pastes, Constr. Build. Mater., 2019, **207**, 672-678.
[17] J. Ren, H. Sun, K. Cao, Z. Ren, B. Zhou, W. Wu, F. Xing, Effects of natural seawater mixing on the properties of alkali-activated slag binders, Constr. Build. Mater., 2021, **294**, 123601.
[18] A.M. Rashad, M.H. Khalil, An investigation of using seawater as mixing water for alkali-activated slag pastes, Innovative Infrastructure Solutions, 2022, **7**(2), 152.
[19] D. Shi, Y. Yao, J. Ye, W. Zhang, Effects of seawater on mechanical properties, mineralogy and microstructure of calcium silicate slag-based alkali-activated materials, Constr. Build. Mater., 2019, **212**, 569-577.
[20] D. Shi, J. Ye, W. Zhang, W. Shen, Damage behavior of calcium silicate slag-based alkali-activated materials exposed to elevated temperatures, Rev. Rom. Mater., 2020, **50**(3), 337-343.
[21] GB/T 1346-2011, Test methods for water requirement of normal consistency, setting time and soundness of the Portland cements, Standardization Administration of China, China, 2011.
[22] GB/T 17671-1999, Method of testing cements – Determination of strength, Standardization Administration of China, China, 1999.
[23] D. Shi, J. Ye, W. Zhang, Effects of activator content on properties, mineralogy, hydration and microstructure of alkali-activated materials synthesized from calcium silicate slag and ground granulated blast furnace slag, J. Build. Eng., 2020, **32**, 101791.
[24] D.L.Y. Kong, J.G. Sanjayan, Effect of elevated temperatures on geopolymer paste, mortar and concrete, Cem. Concr. Res., 2010, **40**(2), 334-339.
[25] E.T. Rodriguez, K. Garbev, D. Merz, L. Black, I.G. Richardson, Thermal stability of C-S-H phases and applicability of Richardson and Groves' and Richardson C-(A)-S-H(I) models to synthetic C-S-H, Cem. Concr. Res., 2017, **93**, 45-56.
[26] N. Yang, W. Yue, The handbook of inorganic metalloid materials atlas (in Chinese), Wuhan University of Technology Press, Wuhan, 2000.
[27] C. Shi, P.V. Krivenko, D. Roy, Alkali-activated cements and concretes, Taylor & Francis, New York, 2006.
[28] X. Lian;, Z. Peng;, L. Shen;, T. Qi;, Q. Zhou;, X. Li;, G. Liu, Properties of low-modulus sodium silicate solution in alkali system, Trans. Nonferrous Met. Soc. China., 2021, **31**(12), 3918-3928.
[29] C.-x. Zhu, Recent advances in waterglass sand technologies, China Foundry, 2007, **4**(1), 13-17.
[30] J. Nordstrom, A. Sundblom, G.V. Jensen, J.S. Pedersen, A. Palmqvist, A. Matic, Silica/alkali ratio dependence of the microscopic structure of sodium silicate solutions, J. Colloid Interface Sci., 2013, **397**, 9-17.

****